# Opportunistic WiFi Spectrum Reuse for Car Density Estimation

Wesam Al Amiri, James T. Jones, Terry N. Guo and Allen B. MacKenzie

Abstract-Signal reuse for multiple purposes is a way to increase spectrum utilization. In this paper, we leverage the WiFi signals of opportunity for the sensing purpose. The spectrograms derived from WiFi downlink (DL) signals reflected from cars are used as fingerprints to efficiently infer car density in parking lots. To achieve this, experimental measurements were conducted in a real outdoor environment to probe the reflected WiFi signals from targets (cars), and the collected datasets are employed for density estimation. The estimator combines hybrid convolutional neural network (CNN) and support vector machine (SVM) for classification, along with least-square estimate (LSE) for interpolation. The probed signals are influenced by many factors, such as the number of WiFi users and data traffic, thereby degrading the estimation accuracy. To address these challenges, we propose an uplink-downlink (UL-DL) WiFi identification and separation technique using the least absolute shrinkage and selection operator (LASSO) technique, without requiring coordination with WiFi access points. Compared to the estimation using a mixture of UL-DL WiFi signals, the simulation results demonstrate that the proposed method achieves significant improvement in estimation accuracy.

Index Terms—WiFi signals of opportunity, signal reuse for spectrum efficiency, uplink-downlink separation, car density estimation, convolutional neural network (CNN), and support vector machine (SVM).

## I. INTRODUCTION

The demand for wireless communication services has been continuously increasing. There have been many growing stresses that call for a revolutionary new spectrum era. One driving philosophy towards the new spectrum era is to further improve spectral efficiency through spectrum reuse in a broader sense. Reusing signals for multiple purposes can achieve even more spectral efficiency. The integration of communication and sensing signals or joint communications and sensing (JCS), for instance, has the potential to provide advanced location and application-aware services with virtually no additional spectrum usage [1]. Intuitively, in addition to the Shannon information (for communication), the Fisher information (for sensing/estimation) can be delivered simultaneously within a certain time over a given spectrum. Various types of communication signals can be reused for sensing applications, such as digital video broadcasting terrestrial (DVB-T) signals [2] and WiFi signals [3].

With the widespread adoption of WiFi devices and the ubiquitous coverage of WiFi networks, WiFi signals have become a valuable resource for sensing the indoor physical environment through various fingerprinting techniques [4]. For

W. Al Amiri, J.T. Jones, T. Guo, and A. MacKenzie are with the College of Engineering, Tennessee Technological University, Cookeville, TN (email: {waalamiri42, jtjones49, nguo, amackenzie}@tntech.edu).

This work is supported by the National Science Foundation under grant #2135275 and by the Center for Manufacturing Research, Tennessee Technological University, Cookeville, TN.

example, in [5], WiFi fingerprints were utilized to detect human presence and classify human activity using SVM by analyzing Doppler information. In another study [6], WiFi fingerprinting and deep learning were employed for indoor 3D localization. Additionally, in [7], WiFi fingerprinting was used as a means to measure building occupancy.

In [8], the authors proposed a machine-based method for indoor-outdoor user detection using WiFi fingerprints. In the field of intelligent transportation systems (ITS), our subsequent work [9] introduced a scheme that reuses the opportunistic spectrum of WiFi signals as fingerprints for estimating car density in parking lots. The proposed scheme provides an efficient and cost-effective alternative to existing parking occupancy detection systems that rely on numerous sensors for real-time occupancy monitoring. Such systems often require substantial implementation and maintenance costs, in addition to the dedicated spectrum usage for data transmission.

In our previous work [9], the car density estimation process utilized a combination of semi-supervised learning and weighted-centroid interpolation techniques to mitigate the reliance on large labeled datasets. The scheme employed the semi-supervised learning to classify opportunistic spectrograms derived from collected WiFi signals under different occupancy scenarios (empty, moderate, and full). Then, the weighted-centroid method was applied to estimate the number of cars in the parking lot. Despite achieving relatively good estimation accuracy, the scheme relies on the power of the collected signals, which is subject to random fluctuations due to the number of active WiFi users and data traffic, as we mentioned in [9]. Furthermore, the weighted-centroid estimator introduces bias, negatively impacting the accuracy of the car density estimation.

To address these problems, in this paper, we propose an effective approach to identify and separate the UL and DL components of the WiFi signal and then apply estimation using the DL signals reflected from targets. This approach aims to remove the strong effects and random fluctuations caused by the varying number of WiFi users and data traffic. It is noteworthy that the UL-DL separation is not straightforward due to the uncontrollable nature of opportunistic WiFi signals and the lack of coordination with WiFi access points (APs). Moreover, the use of time division multiplexing (TDD) by WiFi further complicates the identification process between the UL and DL. Specifically, in the TDD networks, the UL and DL use the same frequency band in different time slots. When viewing such TDD signals on a spectrum display, it is impossible to differentiate the two signals. To tackle this challenge, Wireshark is used to capture and analyze 802.11 packets, which offers valuable insights into the UL-DL packet flow. Simultaneously, we record the reflected WiFi signals

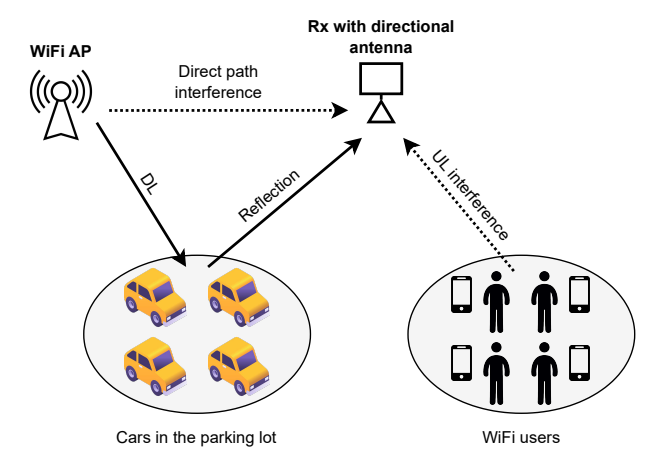


Fig. 1: System description of car density estimation experiment.

using Universal Software Radio Peripheral (USPR) software-defined radios (SDRs). Subsequently, the LASSO technique is employed between a sequence generated using Wireshark information and collected signals in an effort for UL-DL identification and separation. Following that, we employ hybrid CNN-SVM for spectrogram classification and LSE for interpolation to estimate car density in the parking lot. The LSE technique plays a crucial role in mitigating estimation bias and improving estimation accuracy. Finally, simulations were conducted to evaluate the performance of the CNN-SVM model and the LSE. The performance evaluations indicate that car density estimation using spectrograms derived from DL signals can enhance estimation accuracy compared to using spectrograms of a mixture of UL-DL signals.

The rest of this paper is organized as follows. Section II presents system description. The experiment and dataset preparation are presented in Section III. The proposed estimation scheme is described in Section IV. Performance evaluations and numerical results are discussed in Section V, followed by conclusions in Section VI.

#### II. SYSTEM DESCRIPTION

Fig. 1 illustrates the system description of the car density estimation experiment. The system comprises a WiFi AP, a receiver (Rx) equipped with a directional antenna directed to parking lot, a number of cars in the parking lot, and WiFi users.

The WiFi AP broadcasts DL WiFi signals to serve the users within and around the parking lot. The Rx tries to capture reflections from cars for density estimation. However, there is interference due to the direct path between the AP and the Rx, in addition to UL signals from WiFi users. The direct path interference affects the power of spectrograms consistently across different classes. However, this constant level of signal does not actually interfere classification since it does not reduce the distinguishing between classes. For the interference from WiFi users, it needs further signal processing to identify and separate the UL from the captured or recorded signals.

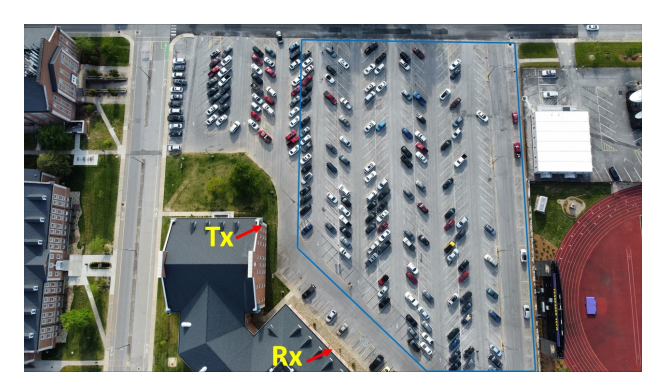


Fig. 2: The environmental layout of Tennessee Tech University parking lot in which the experiment was performed and the locations of the transmitter and receivers used in the experiment.

# III. EXPERIMENT AND DATA SET PREPARATION

# A. Experiment Setup

The experiment setup is shown in Fig. 2, where a USRP used to capture signals from the WiFi AP installed on the wall of Tennessee Tech Library. The heights of the WiFi AP and the USRP Rx are 6 meters. The WiFi AP provides coverage for an area of approximately 8646 square meters, including 282 parking spaces indicated by the blue line in Fig. 2. Signals were collected at 2.421 GHz WiFi frequency band.

Multiple rounds of experiments were conducted to generate datasets that contain car-density information. The desired signals are those reflected by the cars. Nonetheless, several disruptive factors, such as the number of WiFi users and data traffic, affect the strength of collected signals. These factors contribute to the power level of the signals reflected from the target, consequently influencing the density estimation process. In order to mitigate the impact of these disruptive factors, we consider estimation using DL signals reflected from targets. Thus, it becomes essential to differentiate between UL and DL time slots, as they both utilize the same carrier frequency. By isolating the DL slots, the UL slots can be eliminated, while preserving the signal's duration. An approach to differentiate between UL and DL is to utilize Wireshark for packet recording and synchronize it with the signal recorded using the USRP and GNURadio software. Note that Wireshark offers comprehensive details regarding packets, including their source and destination, arrival time, length, data rate, received signal strength indicator (RSSI), and modulation scheme. Fig. 3 (next page) shows information extracted from Wireshark, which has been used to generate a sequence. This sequence can be correlated with the recorded waveform, offering insights into the distinction between UL and DL, as will be explained later.

# B. Signal Post-processing and Uplink-Downlink Separation

Let  $y_{\Sigma}^{(l)}(t)$  be the measured waveform after some process (e.g., time-domain gating and frequency-domain filtering to cut off unrelated parts in the mixed signals), where index l,  $l = 0, 1, \dots, L$ , refers to car density levels of interest, with l = 0 and l = L for empty and full occupant scenarios,

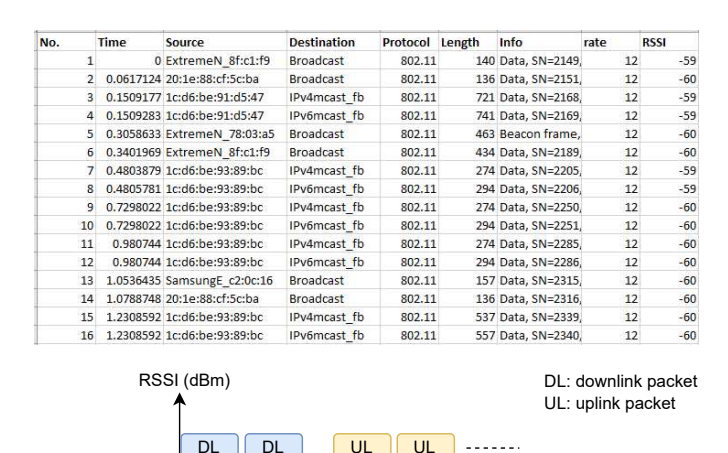


Fig. 3: The information extracted from Wireshark.

respectively. Roughly speaking,  $y_{\Sigma}^{(l)}(t)$  contains three terms and can expressed as

$$y_{\Sigma}^{(l)}(t) = y_{DL,ref}^{(l)}(t) + y_{UL}^{(l)}(t) + y_{bq}^{(l)}(t),$$
 (1)

Time (s)

where  $y_{DL,ref}^{(l)}(t)$  is the DL signal reflected from the cars,  $y_{UL}^{(l)}(t)$  is a sum of all signals caused by UL signal sources, including users' UL signals, the UL signals reflected from the cars, and  $y_{bg}^{(l)}(t)$  account for all background signals and noise, including DL direct-path signal, and DL signal reflected from surrounding clutter. Both  $y_{UL}^{(l)}(t)$  and  $y_{bg}^{(l)}(t)$  are unwanted and considered as interference, but  $y_{UL}^{(l)}(t)$  is much more severer than  $y_{bg}^{(l)}(t)$ . These UL-related signals can be strong if users are close to the probe receiver, and they fluctuate in strength as users move.

To suppress the impact of UL signals, we propose to identify the UL portion from the total received signal  $y^{(l)}_{\Sigma}(t)$  and then remove it. For differentiating UL and DL of the collected signals, we generate virtual vectors (sequences) from Wireshark, which can be stacked into a matrix and used as a dictionary matrix for correlation with the recorded signal. Specifically, for each Wireshark recording, we represent the UL or DL as +1, while no transmission is represented as -1 to create a virtual vector. We denote each virtual vector as  $x_{i_{N\times 1}}$ , and the dictionary matrix as  $\boldsymbol{X}=(x_1,x_2,\cdots,x_i)_{N\times M}$ , where  $i=0,1,\cdots,M$ .

On the other hand, the measured waveform  $y_{\Sigma}^{(l)}(t)$  requires processing, including downsampling, removal of zeros, and cleaning, before being converted into a test vector based on a binary decision or a variable threshold value. In essence, the binary decision or the threshold enforces the waveform's amplitude to be either +1 or -1, with +1 for amplitudes greater than the threshold and -1 for amplitudes less than the threshold. We denote the test vector generated from  $y_{\Sigma}^{(l)}(t)$  as  $y_{N\times 1}$ . It's worth noting that using such values for generating the dictionary matrix and test vector yields desirable correlation results.

After generating the dictionary matrix X and the test vector y, we apply LASSO technique [10] to correlate and align

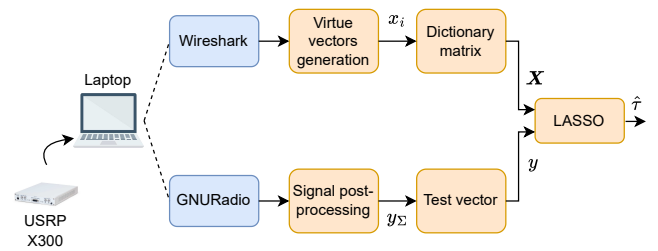


Fig. 4: The proposed concept of estimating the delay between Wireshark and the recorded waveform.

them. Specifically, we estimate the coefficients  $\hat{\beta}$  of the linear regression equation as follows:

$$\hat{\boldsymbol{\beta}} = \underset{\beta}{\operatorname{arg\,min}} \|\boldsymbol{y} - \boldsymbol{X}\boldsymbol{\beta}\|_{2}^{2} + \lambda \|\boldsymbol{\beta}\|_{1}$$
 (2)

where  $\beta \in \mathbb{R}^{N \times 1}$  and  $\lambda$  is a nonnegative regularization parameter. Then, the delay  $\hat{\tau}$  between X and y can be estimated as follows:

$$\hat{\tau} = \Delta t \ index(\max(\hat{\beta})) \tag{3}$$

where  $\Delta t$  is the sampling interval of the waveform. Then, we can shift the Wireshark recording virtual vector  $x_1$  by  $\hat{\tau}$ . Fig. 4 illustrates the steps involved in estimating the delay  $\hat{\tau}$ , which will be employed to align the test vector and virtual vectors. Once the test vector and virtual vectors have been aligned, we can proceed to identify the UL and DL frames within the waveform. When DL is extracted, UL can be deleted (substituting data with zeroes, without changing the signal's duration).

# C. Dataset Generation

For each density level scenario, spectrograms are obtained by applying short-time Fourier transform to  $y_{DL,ref}^{(l)}$ . Specifically, the spectrogram generation process involves dividing the reflected DL signal  $y_{DL,ref}^{(l)}$  into segments, each containing 100,000 samples, which are then transformed into spectrograms. Spectrograms offer a useful representation of the signal, showcasing the relationship between instantaneous frequency and time as a non-negative function. They are also valuable for estimating the power spectral density of the signal, which can be utilized to infer car density.

The spectrograms are utilized as inputs to CNN-SVM that employs image-based classification techniques. This CNN-SVM is trained using the supervised learning algorithm, utilizing 1,610 spectrograms as training inputs. Once trained using spectrograms with known car densities, the CNN-SVM can classify spectrograms of signals with unknown car densities into the predefined classes. Leveraging its learned features and patterns, the CNN-SVM makes predictions and assigns the unknown spectrograms to the appropriate car density class. This classification process, combined with the LSE technique, enables the estimation of car densities.

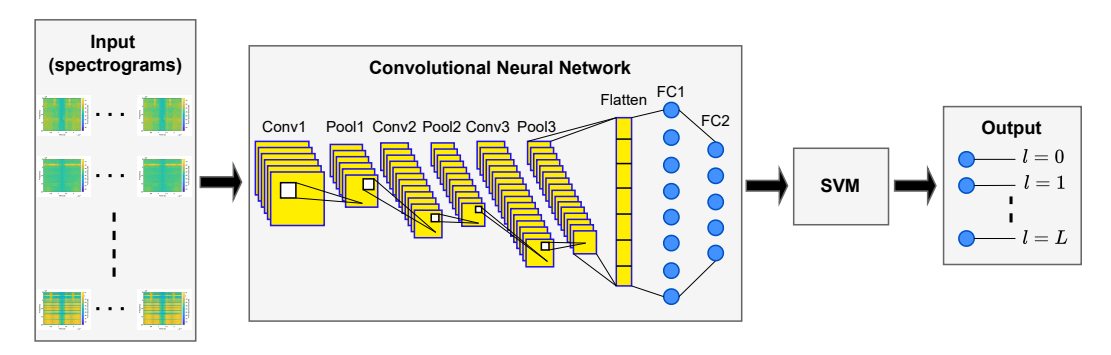


Fig. 5: The structure of the proposed hybrid CNN-SVM classifier.

#### IV. ESTIMATION USING CNN-SVM AND LSE

We employed our CNN architecture, as proposed in [9], and integrated SVM to create the hybrid CNN-SVM, as shown in Fig. 5. This hybrid model combines the key properties of both classifiers, with the CNN functioning as a feature extractor and the SVM as a classifier. It simplifies the CNN architecture to reduce training time and combines the advantages of CNN and SVM to enhance classification accuracy [11], [12]. The CNN-SVM utilizes spectrograms derived from a processed DL WiFi signal obtained through the USRP X310 SDR testbed. For detailed information about the CNN architecture, we refer the reader to [9]. The input to the CNN-SVM consists of multiple segmented sequences of raw IQ samples represented as graphical spectrograms with a size of  $224 \times 224 \times 3$  pixels. These spectrograms are collected at  $L \ (\geq 2)$  different car density levels to train and evaluate the CNN-SVM. Specifically, we considered six car density levels: l = 0 for 8 cars, which is considered as the lowest density level since parking cannot be controlled, l=1 for 52 cars, l=2 for 106 cars, and l=3for 165 cars, l = 4 for 201 cars, and l = 5 for the full density level (i.e., 282 cars).

After collecting the datasets and generating spectrograms, we employ a supervised learning approach with CNN-SVM to train the datasets. The idea is to utilize L labeled datasets with a known number of cars, along with an unlabeled dataset containing an unknown number of cars, which will be classified into the predefined L classes.

Subsequently, the unlabeled dataset can be preprocessed by generating spectrograms for the unknown number of cars. Without considering the labels, the trained CNN model is employed to extract features from the unlabeled spectrograms. Then, the SVM applies a multi-classification between the unlabeled dataset spectrograms and each pre-defined labeled dataset. Finally, the trained CNN-SVM model validates the unlabeled dataset and provides accuracy values against each labeled dataset.

Next, we develop an LSE based car density estimator. Assume there are L training datasets with each being associated with a pre-defined classification level (class). Let  $N_l$  be the actual car density (number of cars) that is associated with the l-th class, and  $\hat{N}$  be the car density estimate; let  $A_j^{(l)}$  be the similarity score of the j-th training dataset against class l, which is the cross-entropy obtained from the classifier; let  $\hat{A}^{(l)}$  represent the similarity score of a testing dataset for an

unknown car density against class l. Define vectors  $\eta$ ,  $\hat{\zeta}$  and  $\zeta_i$ :

$$\eta = (N_0, N_1, \cdots, N_{L-1})^T$$
(4)

$$\hat{\zeta} = (\hat{A}^{(0)}, \hat{A}^{(1)}, \cdots, \hat{A}^{(L-1)})^T \tag{5}$$

$$\zeta_{j} = \left(A_{j}^{(0)}, A_{j}^{(1)}, \cdots, A_{j}^{(L-1)}\right)^{T},$$

$$j = 0, 1, 2, \cdots, L - 1.$$
(6)

Then, form a matrix that is a stack of L accuracy vectors:

$$\boldsymbol{Z} = \begin{pmatrix} \boldsymbol{\zeta}_0^T \\ \vdots \\ \boldsymbol{\zeta}_{L-1}^T \end{pmatrix}_{L \times L} \tag{7}$$

Consider a density estimator expressed as:

$$\hat{N} = \hat{\boldsymbol{\zeta}}^T \boldsymbol{w}, N_i = \boldsymbol{\zeta}_i^T \boldsymbol{w}, j = 0, 1, \cdots, L - 1$$
 (8)

where  $\boldsymbol{w}$  is an unknown  $L \times 1$  weighting vector to be determined. Equations  $N_j = \boldsymbol{\zeta}_j^T \boldsymbol{w}, j = 0, 1, \cdots, L-1$ , can be rewritten in a compact format  $\boldsymbol{\eta} = \boldsymbol{Z}\boldsymbol{w}$  and the weighting vector is given by  $\boldsymbol{w} = \boldsymbol{Z}^{-1}\boldsymbol{\eta}$ . Practically, the training dataset contains multiple measurements for each class, which means we can form a tall matrix  $\boldsymbol{Z}$  with L' rows (L' > L), corresponding to a car density vector  $\boldsymbol{\eta}$  with L' class elements. In such an overcomplete system, the optimal weight can be solved using LSE as follows:

$$\boldsymbol{\omega}^* = \left( \boldsymbol{Z} \boldsymbol{Z}^T \right)^{-1} \boldsymbol{Z} \boldsymbol{\eta} \tag{9}$$

which leads to the following optimal estimator

$$\hat{N}_v = \hat{\boldsymbol{\zeta}}^T \boldsymbol{\omega}^* \tag{10}$$

Note that the LSE serves as an unbiased optimal estimator, in contrast to the weighted-centroid technique proposed in [9]. The weighted-centroid technique with accuracy values as its weights does not guarantee unbiased estimation.

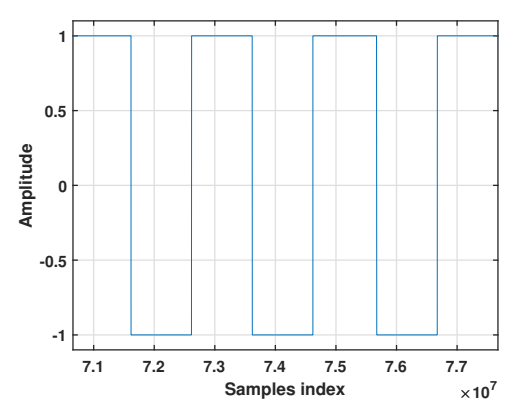


Fig. 6: A segment of a virtual vector generated from the Wireshark.

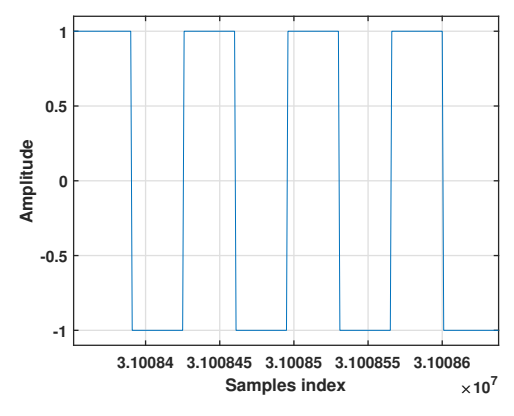


Fig. 7: A segment of the test vector generated from the recorded waveform.

## V. PERFORMANCE EVALUATION

In this section, we assess the effectiveness of the proposed car density estimation method for parking lots. There are L=6 car density levels being considered for evaluation, corresponding to 8, 52, 106, 165, 202, and 282 cars. To evaluate its performance, we use the dataset of l=2 density scenario (i.e. 106 cars dataset) as the testing dataset with an unknown number of cars, while the other training datasets serve as benchmarks for estimating the number of cars.

# A. Analysis of Signal Post-processing and Uplink-downlink Separation

As stated in Subsection III-B, achieving a strong correlation between the Wireshark data and the recorded waveform is essential for identifying the UL and DL components of the recorded waveform. The first step involves generating the sequence based on the information retrieved from Wireshark, as illustrated in Fig. 3. Then, this sequence is transformed into virtual vectors with  $\pm 1$  values and an approximate 50% duty cycle. Fig. 6 shows a segment of the obtained virtual vector.

The second step is to convert the recorded waveform to the test vector with  $\pm 1$  values based on a threshold Th value, which can be computed as follows:

$$Th = \frac{\sum_{k} p_k \nu_k}{2} \tag{11}$$

where  $p_k$  and  $\nu_k$  represent the signal peak and valley, respectively. Fig. 7 shows the test vector generated based on the

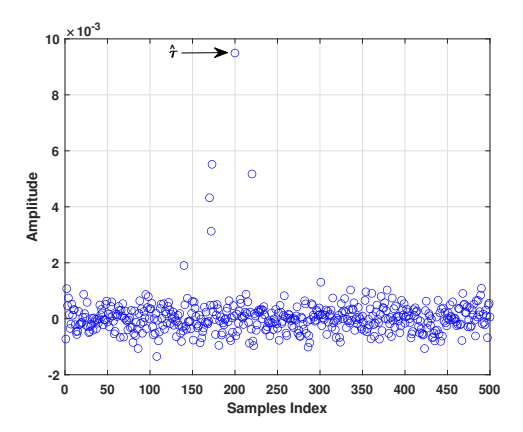


Fig. 8: Correlation result using LASSO technique.

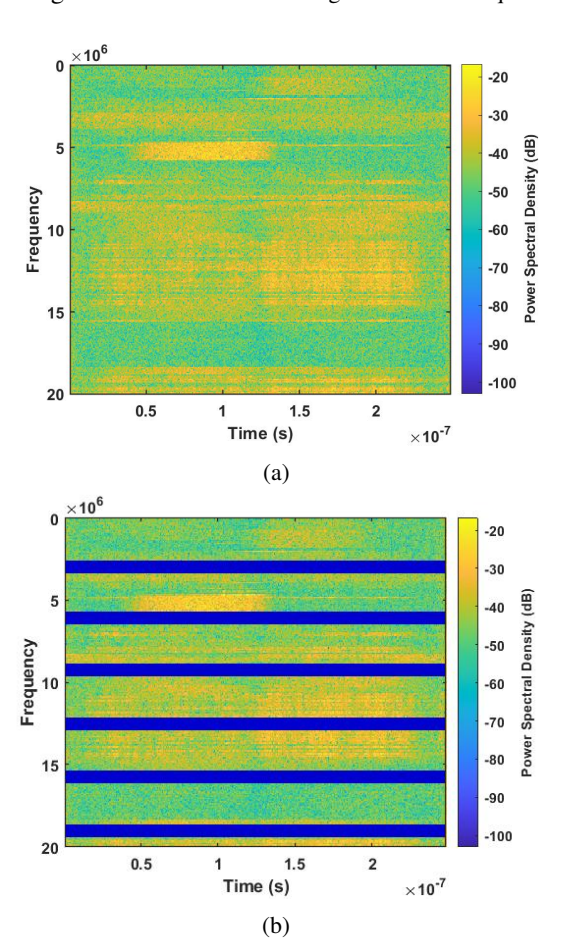


Fig. 9: Spectrogram of a segment of a collected signal: (a) before UL-DL separation, and (b) after UL-DL separation

threshold value. Similar to the virtual vector, the test vector exhibits a 50% duty cycle, approximately.

Finally, after applying the LASSO algorithm, the estimated delay  $\hat{\tau}$  is approximately 200 samples, as depicted in Fig. 8. Then, we can align both the test vector and the virtual vectors and identify the UL-DL of the recorded waveform. Subsequently, both the test vector and the virtual vectors can be aligned, allowing for the identification of the UL-DL components within the recorded waveform.

Fig. 9 shows the spectrogram of a segment of a collected signal before and after performing the UL nulling operation.

TABLE I: Similarity measurements between 106 cars testing class and training classes.

Type of reused signal	8 Cars	52 Cars	165 Cars	201 Cars	282 Cars
DL only	0.0220	0.3521	0.4243	0.1302	0.0714
UL & DL	0.0010	0.2414	0.5000	0.1429	0.1419

The UL signal contains data from WiFi users, affecting the power spectrum density of the spectrograms and reducing the accuracy of density estimation. By removing the UL, we can perform estimation using only DL signals, thereby mitigating the impact of WiFi user data traffic and achieving improved estimation accuracy.

# B. Car Density Estimation Performance Metrics

We assess the performance of the proposed CNN-SVM model by measuring the validation similarity between the testing class with unknown density scenario and the pre-defined training classes. In the evaluation process, we considered the testing data of l=2 (i.e. 106 cars) as input for the CNN-SVM multi-classifier. This was validated against the training data of  $l=0,\ l=1,\ l=3,\ l=4,$  and l=5, corresponding to 8, 52, 165, 201, and 282 cars, respectively. Note that the testing class has never been trained using the CNN-SVM model.

For the performance evaluation of car density estimation using LSE estimator, the estimator is assessed in terms of root mean square error deviation (RMSD).

# C. Numerical Results

To assess the performance of the supervised learning CNN-SVM model, we divided the spectrograms datasets of  $\{8,52,165,201,282\}$  cars into training and testing sets. Then, we used the spectrograms of 106 cars as an unknown dataset for validation. Note that this procedure has been applied to both DL signals after separation and the mixture of UL-DL without separation.

Table I gives the validation similarity between the 106 cars class and the training classes for both DL data and the mixture of UL-DL data. The results indicate that according to the CNN-SVM model, the testing 106 cars class is likely to fall between the 52 and 165 cars classes for both DL and mixture UL-DL scenarios, where the highest similarity values are observed. For instance, in the DL only scenario, the similarity values indicating that the 106 cars class belongs to the 52 cars class and the 165 cars class are 0.3521 and 0.4243, respectively. It's worth noting that the CNN-SVM model does not yield high accuracy values as it hasn't been trained on the 106 cars class.

After evaluating the proposed CNN model, we can apply the LSE estimation method to estimate the number of cars of the 106 cars dataset based on equations (4) – (10). The LSE leads to an estimate of  $\tilde{N}_v=113$  when using DL signals alone, which closely aligns with the actual number of cars, 106. Then, the calculated RMSD of the car density estimator over several iterations is equal to 6.8%, approximately. For the UL & DL mixture scenario, the LSE leads yields an

estimate of  $\hat{N}_v=132$  with an RSMD of 24.9%. One can observe that using the DL signals only can achieve higher estimation accuracy compared to the UL & DL mixture. It can be observed that using DL signals exclusively achieves higher estimation accuracy compared to the UL & DL mixture. This difference is attributed to the mitigation of the influence of the number of WiFi users and data traffic on the classification and estimation process.

#### VI. CONCLUSIONS

In this paper, we proposed and tested a particular use case of reusing the spectrum of DL WiFi signals of opportunity for car density estimation. The proposed scheme exploits spectrograms generated from the WiFi DL signals as fingerprints to provide an efficient and cost-effective alternative to current parking occupancy detection systems. It makes use of the combination of hybrid CNN-SVM for classification and LSE for interpolation to estimate the car density. To mitigate the effect of WiFi users' UL signals on the estimation accuracy, we introduced UL-DL identification and separation method using LASSO technique. The simulation results suggest that proposed UL signal removal technique leads to significant improvement in estimation accuracy. Our preliminary work has demonstrated the promise of low-cost non-coordinated reuse of existing signals for sensing, but further research in this line is still needed to improve the estimation accuracy.

#### REFERENCES

- [1] F. Liu, Y. Cui, C. Masouros, J. Xu, T. X. Han, Y. C. Eldar, and S. Buzzi, "Integrated sensing and communications: Toward dual-functional wireless networks for 6g and beyond," *IEEE Journal on Selected Areas in Communications*, vol. 40, no. 6, pp. 1728–1767, 2022.
- [2] T. Martelli, F. Colone, and R. Cardinali, "DVB-T based passive radar for simultaneous counter-drone operations and civil air traffic surveillance," *IET Radar, Sonar & Navigation*, vol. 14, no. 4, pp. 505–515, 2020.
- [3] W. Li, R. J. Piechocki, K. Woodbridge, C. Tang, and K. Chetty, "Passive WiFi radar for human sensing using a stand-alone access point," *IEEE Transactions on Geoscience and Remote Sensing*, vol. 59, no. 3, pp. 1986–1998, 2020.
- [4] S. Shang and L. Wang, "Overview of WiFi fingerprinting-based indoor positioning," *IET Communications*, vol. 16, no. 7, pp. 725–733, 2022.
- [5] W. Li, B. Tan, and R. J. Piechocki, "WiFi-based passive sensing system for human presence and activity event classification," *IET Wireless Sensor Systems*, vol. 8, no. 6, pp. 276–283, 2018.
- [6] A. Alitaleshi, H. Jazayeriy, and J. Kazemitabar, "EA-CNN: A smart indoor 3D positioning scheme based on Wi-Fi fingerprinting and deep learning," *Engineering Applications of Artificial Intelligence*, vol. 117, p. 105509, 2023.
- [7] J. Bexhorn and K. Kvarnefalk, "Wi-Fi fingerprinting as a mean to measure building occupancy: A case study in an office environment," 2023.
- [8] G. Shtar, B. Shapira, and L. Rokach, "Clustering Wi-Fi fingerprints for indoor–outdoor detection," Wireless Networks, vol. 25, pp. 1341–1359, 2019.
- [9] W. Al Amiri, O. Abdelsalam, J. T. Jones, T. N. Guo, and A. B. MacKenzie, "Signals of opportunity for car density estimation with limited training data," in proc. of IEEE International Symposium on Networks, Computers and Communications (ISNCC), 2023.
- [10] S. L. Kukreja, J. Löfberg, and M. J. Brenner, "A least absolute shrinkage and selection operator (LASSO) for nonlinear system identification," *IFAC proceedings volumes*, vol. 39, no. 1, pp. 814–819, 2006.
- [11] M. O. Khairandish, M. Sharma, V. Jain, J. M. Chatterjee, and N. Jhanjhi, "A hybrid CNN-SVM threshold segmentation approach for tumor detection and classification of MRI brain images," *IRBM journal*, vol. 43, no. 4, pp. 290–299, 2022.
- [12] X. Sun, J. Park, K. Kang, and J. Hur, "Novel hybrid CNN-SVM model for recognition of functional magnetic resonance images," in proc of IEEE International Conference on Systems, Man, and Cybernetics (SMC), 2017.